Characterization and possible hazard of an atypical asbestiform sepiolite associated with aliphatic hydrocarbons from Sassello (Ligurian Apennines, Italy)

Characterization and possible hazard of an atypical asbestiform sepiolite associated with aliphatic hydrocarbons from Sassello (Ligurian Apennines, Italy)

R. Giustetto*[1,2], L. Macaluso[1], G. Berlier[2,3], Y. Ganjkhanlou[2,3], L. Barale[4]

[1]Department of Earth Sciences, University of Turin, via Valperga Caluso 35, 10125 Torino (Italy)
[2]NIS Centre (Nanostructured Interfaces and Surfaces), via Pietro Giuria 7, 10125 Torino (Italy)
[3]Department of Chemistry, University of Turin, via Pietro Giuria 7, 10125 Torino (Italy)
[4]Consiglio Nazionale delle Ricerche, Istituto di Geoscienze e Georisorse, Via Valperga Caluso, 35, 10125 Torino (Italy)

**Corresponding author e-mail: roberto.giustetto@unito.it*

Abstract

An unusual occurrence of asbestiform sepiolite, filling veins in the antigorite serpentinites of the Voltri Unit exposed in a borrow pit (nowadays reclaimed) in the Deiva forest, near Sassello (NW Italy), was probed with an in-depth analytical approach aimed at studying its crystal-chemistry and structure and evaluating its possible hazards for human health. Optical microscopy and SEM-EDS proved that these sepiolite fibres, apparently up to several cm long, are made up of bundles of thinner fibrils (or laths: average length > 100 μm; thickness ≈ 80 nm), with a composition consistent to that reported in the literature. The dehydration process was monitored through TGA and FT-IR, performed at increasing *T*; the latter, in particular, evidenced the presence of moderate amounts of aliphatic hydrocarbons – not yet thoroughly identified – somehow associated to the sample. The crystal structure refinement with the Rietveld method showed no relevant difference from the literature models, although a peculiar distribution of zeolitic H_2O molecules was observed. The geological context suggests that the Sassello sepiolite precipitated from hydrothermal fluids, which were saturated in Mg and silica by the interaction of the host serpentinites. The same setting favoured formation of abiotic hydrocarbons, by means of the Fischer-Tropsch reaction. The extremely long and flexible fibrils (length/width aspect ratio >> 3) of this sepiolite specimen could represent a serious hazard for human health if air dispersed and

breathed; also, its atypical association with hydrocarbons (only reported once previously) might even favour further fragmentation in thinner units.

Keywords: sepiolite, aliphatic hydrocarbons, Fischer-Tropsch-type reaction, hydrothermal system, noxiousness hazard.

1. Introduction

Sepiolite [ideal formula: $Mg_8Si_{12}O_{30}(OH)_4(OH_2)_4 \bullet 8H_2O$] is a natural occurring microporous clay mineral, belonging to the palygorskite/sepiolite group and originating in a wide variety of geological environments. Some occurrences derived by direct precipitation from highly-saline waters, or from alteration of other clay minerals, in lacustrine and marginal-marine settings, under semi-arid to arid climatic conditions (Eugster and Hardie, 1975; Trauth, 1977; Weaver, 1984; Velde, 1985; Jones and Galán, 1988; Chahi *et al*., 1997; Mayayo *et al*., 1998; Galán and Pozo, 2011); authigenesis in calcareous soils under semi-arid conditions has also been reported (Galán and Pozo, 2011). Other known occurrences originated after seafloor hydrothermal alteration of basaltic glass, volcanoclastic and clayey sediments, or ultramafic rocks (e.g., Bonatti *et al*., 1983; Bach *et al*., 2002). Sepiolite can also form in on-land hydrothermal systems by precipitation from low *T* (< 100°C) Si/Mg enriched fluids circulating in different rock types, including carbonate rocks (Ehlmann *et al*., 1962; Imai and Otsuka, 1984; Kovács-Pálffy *et al*., 2016) and ultramafites/meta-ultramafites (e.g., Yalçin and Bozkaya, 2004). A biogenic origin induced by microorganisms (Leguey *et al*., 2010; Cuevas *et al*., 2012; del Buey *et*

al., 2018) was also reported. In the crystal structure of sepiolite (Brauner and Preisinger, 1956; Brindley, 1959), the octahedral (O) layer splits into ribbons elongated in the *z*-axis direction and pinched between two continuous, 'waving' tetrahedral (T) sheets, due to a periodic inversion in the apical oxygens orientation. Chessboard connected TOT ribbons alternate to nano-tunnels (maximum effective width: 10.6 Å), running along *z* and filled by weakly bound zeolitic H_2O (Ferraris *et al*., 2008). Tightly bound, structural OH_2 (Bailey *et al*., 1980) completes the coordination of octahedral Mg at the ribbon borders. Exchangeable ions and/or small molecules may be hosted within the tunnels and/or on the fibre surface.

Due to its nano- and micro-porosity, sepiolite has excellent sorption properties and wide surface area, which can be exploited in a broad variety of applications such as lubricants, catalysts, adsorbents, cleaning compresses for restoration and cat litters (Àlvarez *et al*., 2011; Lòpez-Galindo *et al*., 2011). Moreover, its markedly fibrous habit grants its use as an asbestos substitute in building and seal materials, friction compounds for automotive brakes and high temperature insulators (Solebello, 2009). Sepiolite has been mined for centuries: over 90% comes from Spain (Neogene lacustrine sequences of the Madrid basin; Brell *et al*., 1985; Ordoñez *et al*., 1991), with 800 thousand tons annual production (O'Driscoll, 1992); smaller deposits are located in the USA (Amargosa Desert), Kenia and Tanzania (Amboseli), China (Guanshan), Greece (Ventzia basin) and Somalia (El Bur) (Galán and Pozo, 2011). All commercially sold sepiolites have fibres < 5 μm long (at times, achieved after preliminary grinding) – the threshold of non-carcinogenicity fixed by the International Agency for Research on Cancer, World Health Organization (IARC, 1997). However, sepiolites with unusually long fibres (> 10 μm, due to variability in

the crystallinity degree and texture; Suárez and García-Romero, 2012; García-Romero and Suárez, 2013) have been seldom signaled for their carcinogenic potential (Pott *et al*., 1990; Pott *et al*., 1991; Bellman *et al*., 1997; Giustetto *et al*., 2014). This study describes an atypical asbestiform sepiolite, with extremely long fibres, associated with small amounts of aliphatic hydrocarbons. Similar samples have been seldom reported in the outcropping rocks of Northwestern Italy (e.g., Valle d'Aosta, Piemonte and Liguria: Belluso and Sandrone, 1989; Belluso *et al*., 1995) – only once associated to hydrocarbons (Giustetto *et al*., 2014).

2. **Experimental**

2.1 *Materials and geological setting*

The studied specimen was collected in 2010 by Giuseppe Pipino in a small 'borrow pit' in the Deiva forest (~44°28'42.6"N 8°28'48.1"E, Sassello municipality, Liguria, NW Italy), belonging to the Beigua Geopark (Fig. 1).

(INSERT FIGURE 1)

The Sassello area is located on the northern side of the Ligurian Apennines, and belongs, from a geological point of view, to the Alps-Apennines interference zone *sensu* Piana *et al*. (2017), made up of geological units that shared, at least in part, the evolution of both orogens (Molli *et al*., 2010 and Piana *et al*., 2017, with references therein). This sector is composed of metamorphic rocks derived from the Mesozoic Liguria-Piemonte oceanic domain, presently cropping out in the so-called Voltri ophiolitic 'massif' (Fig. 1).

The Voltri Unit, which underwent eclogite-facies Alpine peak metamorphism, makes up the greatest part of the Voltri 'massif', including the Sassello area. It is composed of lherzolites largely transformed into serpentinites ('Bric del Dente' serpentinite), associated to hm- to km-sized bodies of metagabbro . These are followed by rocks derived from original basalts and basaltic breccias and the relevant metasedimentary cover (Chiesa *et al*., 1975; Piccardo, 1984; Messiga and Scambelluri, 1991; Capponi and Crispini, 2008). To the north, the metamorphic rocks of the Voltri Unit are overlain by the Cenozoic succession of the Tertiary Piemonte Basin. (Capponi *et al*. 2013; d'Atri *et al*. 2016; Federico *et al*., 2016).

This Unit underwent a polyphase tectono-metamorphic evolution (Capponi and Crispini, 2002, 2008). Subduction-related, eclogite facies Alpine metamorphism was followed by a diffuse re-equilibration in greenschist facies during exhumation phases, associated to two superimposed phases of isoclinalic to tight folding (D1 and D2), which generated the composite, transpositive regional foliation. The D3 phase took place under greenschist to sub-greenschist facies conditions, generating metre- to decametre-scale open folds. The later D4 phase generated gentle to open folds (hm to km wavelength), associated with reverse faults and shear zones that also affected the Oligocene units of the Tertiary Piemonte Basin (Capponi *et al*., 2001; Federico *et al*., 2016) and were sealed by Burdigalian deposits (d'Atri *et al*., 1997; Piana *et al*., 1997). Faults and shear zones related to the D4 phase, as well as younger E-W and NW-SE trending fault systems, hosted a polyphase fluid circulation accompanied by complex rock-fluid interactions, causing local metasomatic alterations of host and fault rocks and precipitation of various vein minerals (Piana *et al*., 2006; Spagnolo *et al*., 2007).

(INSERT FIGURE 2)

The quarry of collection of the investigated sepiolite was positioned West of the Sassello village, and was open in the 'Bric del Dente' antigorite serpentinites, close to the contact with the sediments of the Tertiary Piemonte Basin (Fig. 2). The quarry, completely decontaminated after the finding of asbestiform minerals, is nowadays no more accessible. In this locality, sepiolite occurred as a fibrous, yellow-to-whitish mineral, showing a slip-fibre growth in cm-thick and dm-long veins, associated with minor calcite. The studied specimen was purified before analyses, by manually removing the contaminant phases (mostly serpentine, derived from vein walls, and calcite) under a stereomicroscope. The residual fraction was dispersed in deionized water, isolating the lighter suspended portion from the heavier residual impurities (Giustetto and Chiari, 2004). Purified samples were hand-ground in an agate mortar and powdered; conventional X-ray diffraction proved sepiolite to be the only detectable phase.

2.2 Methods

Polarizing microscopy was performed on 30 μm thin sections by using a Zeiss WL Pol optical polarizing microscope; Scanning electron microscopy (SEM) with a JEOL JSM IT300LV (EHT 20 kV, working distance 10 mm; High Vacuum – Low Vacuum 10/650 Pa - 0.3-30kV). Chemistry was obtained by electron probe microanalysis (EPMA), using an EDS Oxford INCA Energy 200, equipped with an INCA X-act SDD Thin Window detector, for detection of light elements down to Boron. The samples, coated by a 5 nm thick Au layer to allow conductivity, were

attached to step brass stubs to allow examination of the fibres. Due to the difficulties in analyzing fibrous samples, chemical analyses were collected on 10 x 10 μm^2 areas on a pressed, sintered and carbon-coated sepiolite pellet, obtained with a press designed to prepare IR-spectroscopy samples (operating conditions: 50 s counting time, 15 kV accelerating voltage, 25 mm working distance, 300 pA beam current). The collected data were processed with the Microanalysis Suite Issue 12, INCA Version 4.14 and calibrated on natural mineral standards using the ZAF correction method. The weight % sums of oxides, showing no relevant heterogeneity, were averaged to obtain a reliable crystal-chemical formula.

Thermo-gravimetric analyses (TGA) were performed on ≈ 10 mg specimen in an alumina crucible, using a simultaneous TGA/DSC (Differential Scanning Calorimetry) TA Instruments Q600, both in nitrogen and Ar flows (100 mL/min), from room *T* to 1000 °C following a 10 °C/min ramp. DSC data were obtained through the temperature difference between the sample pan and a reference pan.

For Fourier-Transform Infra-Red (FTIR) measurements, ≈15 mg of the material was pressed into a self-supported pellet, few μm thick, and placed in a small golden folder inside a commercial FT-IR reactor cell (AABSPEC, no. 2000-A multimode), which allows recording of IR spectra under controlled temperature and gas atmosphere. FTIR spectra were recorded in transmission mode with a resolution of 2 cm^{-1} on a PerkinElmer System 2000 infrared spectrophotometer, equipped with a MCT detector at liquid nitrogen temperature. Two different sets of data were collected: i) at room *T*, under He flow for 1 h; ii) progressively heating from room *T* until 400 °C, with a ramp of 10 °C/min in a He flow (50 cc/min).

Synchrotron XRPD data were collected at room *T* at the European Synchrotron Radiation Facility (ESRF) in Grenoble (France), on the ID22 High-Resolution Powder-Diffraction beamline, using a wavelength of $\lambda = 0.400016(2)$ Å. The specimen was loaded into a 1 mm diameter, spinning glass capillary, in order to limit preferred orientation effects. Collection time was 120 sec. Diffracted beams were collected by a bank of nine detectors mounted on a single rotation stage (Hodeau *et al*., 1998), each preceded by a Si 111 analyser crystal, scanned vertically to measure the diffracted intensity as a function of 2θ, accessing d-values from 0.774 to 22.650 Å. The GSAS software package (Larson and Von Dreele, 2007) and the EXPGUI graphical user interface (Toby, 2001) were used for Rietveld refinement. Background was fitted using a 24-term shifted-Chebyshev function and peak profiles modelled with a pseudo-Voigt function as parameterized by Thompson *et al*. (1987), with asymmetry corrections according to Finger *et al*. (1994). Initially, only the background, scale factor, zero and unit-cell parameters were refined. Later, fractional coordinates were refined for all atoms and occupancy factors for structural OH_2 and zeolitic H_2O, at first in alternate cycles (to minimize correlations) and finally at once. Soft constraints were imposed on tetrahedral and octahedral bond lengths and angles and progressively reduced; only the lower weighting factor (F = 10) yielding reasonable bonds lengths was kept, in order to avoid unrealistic polyhedrons distortions (Post *et al*., 2007; Post and Heaney, 2008; Giustetto *et al*., 2011a; Giustetto and Compagnoni, 2011; Giustetto *et al*., 2014). Isotropic displacement parameters (Uiso) for all atoms were adjusted using overall constraints for each chemical species. Residual preferred orientation for the (110) reflection, though attenuated by capillary data collection, was treated with the

March-Dollase model (March, 1932; Dollase, 1986). The consistency of the refined model was constantly monitored by checking the Goodness-Of-Fit parameters and the fit between the observed and calculated profiles; structural reliability was monitored with the 'Moldraw' software (Ugliengo *et al*., 1993).

3. **Results and discussion**

3.1 Macroscopic observation, stereomicroscopy in reflected light, polarizing microscopy and scanning electron microscopy with microprobe analysis

(INSERT FIGURE 3)

Even to the naked eye, the asbestiform habit of the Deiva forest sepiolite is manifest (Fig. 3). Macroscopically, long and apparently thick fibres (from 5 mm up to 6-7 cm) are observed, often grouped in bundles, classifiable to the V group according to García-Romero and Suárez (2013; see Fig. 2 therein). These fibres are flexible, cream to light brown in colour and readily split into thinner units when manipulated, usually crystallizing parallel to the vein selvages (slip type), with a thickness from < 1 to several mm. The minerals of the palygorskite/sepiolite group are sometimes known to form compact and soft cardboard-like felts ('mountain leather': Grim, 1968; Frost *et al*., 1998; Imai and Otsuka, 2000), in which tangled fibres form an apparently continuous mat. Asbestiform occurrences, however, have also been reported (Giustetto and Compagnoni, 2011; Giustetto *et al*., 2014). Observation under the stereo-microscope confirms that these long fibres are bundles of thinner fibrils, intricately intergrown and separable by sheer mechanic

stress. Polarizing microscopy on thin sections (≈ 30 μm), cut parallel to the fibres elongation, shows a slight brown-to-yellowish pleochroism. The first colour occurs when the fibre elongation runs parallel to the polarizer, implying that γ (higher refraction index) runs parallel to *z*. The α and β orientation, perpendicular to the fibres elongation, could not be determined. In crossed-nicols, a symmetrical extinction is observed, consistently with the orthorhombic symmetry of this phase. High and various interference colours are seemingly observed in different areas – an effect caused by the difficulty in obtaining thin sections with a constant thickness for fibrous materials. Determination of the correct interference colour is risky, but the predominance of higher ones tends to suggest moderate birefringence. Conoscopic light confirms that the mineral is biaxial, with a positive optical sign.

Morphological analysis performed by SEM confirm that the cm-long fibres are indeed aggregates of thinner units (*fibrils* or *laths*, García-Romero and Suarez, 2014), mainly running parallel and often entangled (Fig. 4.a). Fine measurements of their dimensions (Fig. 4.b) evidenced an average thickness of ≈ 83 nm and lengths > 100 μm (IV group: very long fibres: García-Romero and Suárez, 2013). SEM observations also proved that their flexibility affects the micrometric scale.

(INSERT FIGURE 4)

(INSERT TABLE 1)

The chemical composition resulting from EDS spot analyses (Table 1) is consistent with previous data (Garcia-Romero and Suàrez, 2010; Suàrez and Garcia-Romero, 2011; Giustetto *et al*., 2014). Si and Mg are the main components, together with moderate Fe substituting for Mg in octahedral coordination. Scarce Al (Al_2O_3 < 0.05 wt. %) suggests for this sepiolite an almost exclusively tri-octahedral

character. Sum of oxides varies within 81 and 85 %, consistently with the hydrous content detected by thermogravimetry (see section 3.2). Low exchangeable ions amounts (Na^+ and K^+), possibly located inside the tunnels, are at times detected.

On an anhydrous basis, the crystal chemical formula $Si_{12,13}O_{32}(Mg_{6,47},Fe_{0,84})_{\Sigma 7,31}$ (total iron as Fe^{3+}) was obtained. The slight Si excess with respect to the ideal value (12) may be explained by the presence of small amounts of amorphous silica (Karakaya *et al*., 2011; Giustetto *et al*., 2014). The rather low octahedral content (< 8), not rare in sepiolite, is consistent with the amount of Fe^{3+}, as well as the presence of vacancies (Suàrez and Garcia-Romero, 2011; Giustetto *et al*., 2014).

3.2 Thermogravimetric analysis

(INSERT FIGURE 5)

TGA/DSC data collected on the Deiva forest sepiolite are reported in Fig. 5. All weight losses and thermal events, related to the loss of the hydrous content, are consistent with previous studies (Nagata *et al*., 1974; Ruiz *et al*., 1996; Weir *et al*., 2002). In sepiolite, correlations between TGA features and structural changes are known not to be straightforward, as no strict partitioning exists between the loss of different kinds of water (Mifsud *et al*., 1987). Reasonable interpretations, however, can be drawn. All main events and related attributions are detailed in Table 2.

A significant weight loss is observed between room *T* and 120 °C (≈ 8 %), related to the departure of pellicular, physisorbed water (from the fibre surface) and of zeolitic H_2O positioned at the edges of the tunnels. Such a loss is consistent, albeit slightly lower, with literature data (10-11 wt. %, as observed by Jones and

Galan, 1988; Frost and Ding, 2003). A similar decrease was recently observed on a similar sepiolite occurrence (Giustetto *et al*., 2014) and attributed to the presence of small amounts of hydrocarbons on the fibre surface, which may possibly limit the adhesion of pellicular water. A further weight loss (≈ 4.5 %) occurs until 310 °C, due to the departure of the residual zeolitic H_2O together with the first fraction of structural OH_2. Loss of the remaining OH_2 (3.5 %) and following dihydroxylation (2.5 %) proceed until 790 °C, when clinoenstatite (or an amorphous phase) appears. The overall weight loss (≈ 18.5 %) is similar to that recorded in the literature (i.e., 18.5-19.5 %: Frost *et al*., 2009; Giustetto *et al*., 2011c).

(INSERT TABLE 2)

3.3 Fourier Transform IR spectroscopy

(INSERT FIGURE 6)

The collected FT-IR patterns are basically consistent with literature data (Frost *et al*., 2001; Ovarlez *et al*., 2009; Bukas *et al*., 2013), although slight shifts in positions might depend on different environments due to crystal-chemical compositions (Ahlrichs *et al*., 1957) or to the strength of H-bonds between OH_2 and H_2O (Mendelovici, 1973; Mendelovici and Portillo, 1976; Giustetto *et al*., 2011b). A detailed attribution of the sepiolite vibrational modes and their evolution with He flux and *T* rise is reported in Table 3.

FT-IR spectra were first collected at room *T* in He flow for 1 h, to induce a gradual loss of the more weakly bound H_2O molecules at a constant temperature. In these spectra, three main signals appear in the stretching region (Fig. 6, left-hand

side) at 3246, 3350 and 3582 cm^{-1}, followed by another one at 3680 cm^{-1}. The former two – related to physisorbed and zeolitic H_2O, respectively – gradually decrease as the He flow proceeds; the latter two maintain their position and intensity throughout all the experiment duration, consistently with the permanence in the framework of structural OH_2 and hydroxyls in the O sheet, respectively. As dehydration proceeds, two faint bands appear at 3207 and 2925 cm^{-1}: these bands should not be related to sepiolite, but rather to tiny amounts of aliphatic hydrocarbons. In the bending region (Fig. 6, right-hand side), two similar bands appear at 1658 and 1620 cm^{-1}, related to physisorbed/zeolitic H_2O and Mg-coordinated OH_2, respectively (Hayashi *et al*., 1969). In time, these signals tend to coalesce forming a narrow doublet (1622 and 1614 cm^{-1}), mainly related to OH_2. A significant change affects the 1209 cm^{-1} signal, which red-shifts at 1192 cm^{-1} after treatment, thus suggesting its dependence from the mineral hydrous content. A faint signal at 1428 cm^{-1} shows no apparent change with dehydration; again, this band should not be related to sepiolite, but rather to the presence of modest amounts of hydrocarbons (Giustetto *et al*., 2014).

The specimen was then heated from room *T* to 400 °C under the same He flow, to study the consequent structural changes and dehydration steps. A general loss in intensity is observed throughout the entire spectrum, consistently with the further loss of the hydrous fraction (residual zeolitic H_2O and some structural OH_2). In the stretching region (Fig. 7, left magnification), the broad band centered at approximately 3582 cm^{-1} progressively decreases and splits, revealing three separate maxima (3528, 3597 and 3654 cm^{-1}) all related to the ν-OH of structural OH_2. The band related to hydroxyls in the O sheet (3680 cm^{-1}) slightly red-shifts at

3673 cm^{-1}, while a new weak feature appears at 3688 cm^{-1} (left inset of Fig. 7). This splitting accounts for structural folding after formation of di-hydrated sepiolite (SEP $2H_2O$), due to partial loss of structural OH_2 (Hayashi *et al*., 1969; Ovarlez *et al*., 2011); the remaining OH_2 gets closer to the hydroxyls, exerting a mutual H-H repulsion (Serna *et al*., 1975). The same situation is confirmed by the blue-shift of the narrow band at 3720 cm^{-1}, related to Si-OH stretch (Cannings, 1968; Jung and Grange, 2004; Ovarlez *et al*., 2009), which reaches 3736 cm^{-1} at 400 °C. The persistence of the two maxima at 3597 and 3528 cm^{-1} (assigned to OH_2 anti-symmetric and symmetric stretching frequencies, respectively), confirms that at 400 °C some structural OH_2 still occupies the framework. It is relevant that two weak features, positioned at 2925 and 2858 cm^{-1} (asymmetric and symmetric stretching of methylene groups, respectively; Fig. 7), become more and more evident with *T* increase. Again, these bands are not related to sepiolite, but rather to the CH_2 stretch of small amounts of aliphatic hydrocarbons. The band at 3207 cm^{-1}, possibly also related to organic compounds, tends instead to decrease with *T* rise.

(INSERT FIGURE 7)

In the bending zone (Fig. 7, right hand side), heating from room *T* to 400 °C causes the abovementioned narrow doublet to recoalesce in a single peak [structural OH_2 δ(OH): 1620 cm^{-1}], which decreases in intensity as *T* increases, consistently with loss of OH_2 and structure folding. The component at 1192 cm^{-1} almost disappears at 400 °C, implying that such a feature, rather than being related to framework stretching modes (Si-O stretch; Frost *et al*., 2001), could be linked here to the up-warded γ mode of some residual zeolitic H_2O (Giustetto *et al*., 2011b). The weak hump at 1428 cm^{-1} tends to break down in two separate features as *T*

rises (Fig. 7, right-hand magnification), at 1404 and 1456 cm^{-1} respectively; besides, a narrower mode appears at 1509 cm^{-1}. All these bands correspond to similar ones detected on gabbroid or serpentinized-carbonated mantle-derived ultramafic xenoliths or saponite clays of hydrothermal origin, typical of aliphatic hydrocarbons (Ciliberto *et al*., 2009; Sciré *et al*., 2011; Manuella *et al*., 2012). While in the bending region (~1200-1600 cm^{-1}) the bands related to organic matter might be overlapped with overtone of skeletal bands of sepiolite (or oxides) and structural OH groups, this not expected to occur in the stretching zone (~2600-3100 cm^{-1}). In the studied case, those signals appearing in both the stretching and bending regions of organic compounds (i.e., observed at 1404, 1428, 1456 and 1509 cm^{-1}, coupled to those at 2925, 2858 and 3207 cm^{-1}; Table 3), and the related intensity changes, indicate that they can reasonably be ascribed to hydrocarbons.

(INSERT TABLE 3)

3.4. Crystal structure refinement

It is well known that the structural refinement of sepiolite – a highly defective clay mineral with fibrous habit, modest crystallinity and unequal grain size – is troublesome (Krekeler and Guggenheim, 2009; Guggenheim and Krekeler, 2011). All past results, based on synchrotron data of powdered specimens, with broad diffraction peaks and convoluted background (Post *et al*., 2007; Giustetto *et al*., 2011a, 2014), were affected by low accuracy (i.e., one order of magnitude higher than those typical of single-crystal refinements; Guggenheim and Krekeler, 2011). Only Sanchez del Rio *et al*. (2011) presented pioneering XRD data collected on

single-crystals. The crystal structure of the Sassello sepiolite was refined with the Rietveld method on synchrotron powder XRD data. Starting fractional atomic coordinates were taken from Giustetto *et al*. (2014), in view of the apparent analogies between the analyzed specimens. The octahedral (O) sheet was considered occupied only by Mg, ignoring the subordinate Fe content (see Section 3.1) as well as the tiny amounts of exchangeable ions in the tunnels.

Reasonable results in the Rietveld refinement of this highly defective mineral often involve fixing (or constraining) some atomic parameters (Guggenheim and Krekeler, 2011). The positions and occupancies of zeolitic H_2O and structural OH_2 were refined on the entire pattern (Fig. 8) – thus including the stronger (110) reflection at lower angles ($d_{110} \cong 12.1$ Å), symptomatic of the channel content (Ovarlez *et al*., 2009). Once such a procedure converged, this reflection – marked by strong asymmetry – was excluded (an expedient already adopted by Chiari *et al*., 2003; Post *et al*., 2007; Post and Heaney, 2008; Giustetto *et al*., 2011a, 2014) and the atomic coordinates and occupancy factors were blocked for any kind of water . The refinement was then resumed in the 2.5-50 2-Theta degree interval, by adjusting the fractional coordinates of all residual atoms in the structure. Such a protocol allowed obtaining reliable structural data on the polyhedrons sites, while preserving realistic positions and occupancies for all kinds of water (Guggenheim and Krekeler, 2011). The observed and calculated XRPD patterns for the Sassello sepiolite – and related difference curve, are shown in Fig. 8 [in the magnification: excluding the (110) reflection]. Final refinement data, agreement factors and unit-cell parameters are listed in Table 4. Atomic fractional coordinates, occupancy factors and displacement parameters are reported in Table 5. The related ‘CIF’ file

was deposited with the Principal Editors of Mineralogical Magazine and is available from the online version of the journal at https://www.cambridge.org/core/journals/mineralogical-magazine. Despite all the above mentioned limitations, the standard deviations on atomic coordinates are quite low, compared to literature data. Fig. 9 shows the refined structural model.

(INSERT FIGURE 8)

(INSERT TABLE 4)

No spurious experimental reflection, not envisaged by the simulated pattern, was observed during refinement, thus confirming the reliability of the adopted sepiolite structural model (something recently called into question for palygorskite; Garcìa-Rivas *et al*., 2017). Although the goodness of fit is affected by the disorder and multiple defects affecting this and similar clay minerals (Giustetto and Chiari, 2004; Krekeler and Guggenheim, 2009), the quality of the refined model is consistent with previous works (Artioli and Galli, 1994; Chiari *et al*., 2003; Post *et al*., 2007; Post and Heaney, 2008; Giustetto *et al*., 2011a, 2014). Without discussing the finer structural details (something prevented by the relatively high *sigma*s), the unit cell parameters are consistent with previous models (i.e., Post *et al*., 2007; Giustetto *et al*., 2011a, 2014) – the related differences varying within 0.01 Å. Structural OH_2 has an almost full occupancy [0.92(2)]. The occupancy of the 'ZW12' H_2O molecule dropped to zero while refining (Table 5), proving this site to be empty. Such an absence, however, does not affect the global zeolitic H_2O content: almost 16.7 H_2O molecules occupy the unit cell – slightly exceeding the value expected by the ideal formula (16; Preisinger, 1959). A continuous web of H-bonds connects all water molecules among them and to the structural OH_2 (Fig. 9):

the mutual O···O distances in the tunnel vary between 2.271 and 2.765 Å (Jeffrey, 1997). The detection, in the XRD pattern, of broad humps centred at approximately 6.5 and 17.0 2-Theta degrees, though also related to technical issues (i.e., use of a glass capillary during data collection), suggests possible presence of an additional amorphous phase – presumably silica , as hinted by EDS analyses (section 3.1).

(INSERT FIGURE 9)

(INSERT TABLE 5)

3.5. Genesis of the Sassello sepiolite and origin of the associated aliphatic hydrocarbons

The occurrence of sepiolite in the serpentinites of the Voltri Unit was also reported by Spagnolo *et al*. (2004, 2007), who observed this mineral to form mm- to cm-thick "*layers*", genetically related to fluid circulation both in reverse shear zones, associated to the earliest Miocene D4 deformation event, and within post-Burdigalian transtensives and strike-slip fault systems (see section 2.1).

It can be reasonably supposed that the studied asbestiform sepiolite is related to the same genetic context, i.e., a low-temperature hydrothermal circulation that developed along late-orogenic tectonic structures. However, the structural relationships of the sepiolite veins could not be investigated during sampling nor later, due to reclamation of the borrow pit where the mineral had been found.

Mg and Si probably derived from aqueous fluids with negligible Al activity, interacting with serpentinites and partly serpentinised peridotites; Fe from interaction with iron-bearing minerals (e.g., magnetite in serpentinites or olivine

and clinopyroxene in peridotites). A slight SiO_2 excess in solution, which is expected to favour sepiolite precipitation (Birsoy, 2002), may explain the tiny quantities of amorphous silica hinted by the crystal-chemical formula (section 3.1).

The studied sepiolite is associated with long-chain aliphatic hydrocarbons. The abiotic genesis of these organic compounds after hydrothermal activity in mafic to ultramafic rocks has been reported from different geological settings (Charlou *et al*., 1998; Proskurowski *et al*., 2008; Ciliberto *et al*., 2009; Dos Anjos *et al*., 2010; Sciré *et al*., 2011; Etiope and Sherwood Lollar, 2013), and documented to occur even at great depth during subduction of ophicarbonates (Vitale Brovarone *et al*., 2017). Their generation is commonly interpreted as the result of the Fischer-Tropsch-type (FT-t) reaction (MacDonald and Fyfe, 1985; Taran *et al*., 2007; Konn *et al*., 2009), an exothermic reduction of CO and CO_2 by gaseous H_2, catalysed by group VIII ions (such as Fe, Co, Ni) or oxides. C oxides mainly derive from mantle CO_2 dissolved in hydrothermal fluids or liberated from olivine fluid inclusions; H_2 after the hydration of peridotite minerals during serpentinization (Charlou *et al*., 2002; Ciliberto *et al*., 2009; Marcaillou *et al*., 2011).

Considerable amounts of hydrocarbons (mostly methane, with minor ethane and propane) are released by present-day alkaline, Ca-OH springs from the Voltri ophiolitic 'massif' (Bruni *et al*., 2002; Cipolli *et al*., 2004; Boschetti *et al*., 2013; Chavagnac *et al*., 2013; Schwarzenbach *et al*., 2013), which discharge fluids from meteoric waters modified by the prolonged interaction with the host serpentinites and peridotites (Bruni *et al*., 2002; Cipolli *et al*., 2004; Boschetti *et al*., 2013). These hydrocarbons, mostly of abiotic origin (as indicated by the C and H isotopic compositions), formed during low-temperature serpentinization of the host

ultramafic rocks by the same meteoric-derived fluids, either through FT-t reactions or direct production of CH_4 (without intermediate H_2 generation) by CO_2-rich fluids (Boulart *et al*., 2012; Boschetti *et al*., 2013).

Bruni *et al*. (2002) modelled the reaction path of meteoric waters with Voltri serpentinites and proposed a two-step evolution, in which Ca-OH waters are formed by low-temperature interactions with the host rocks, passing through an intermediate Mg-HCO_3 composition (springs with this composition are also common in the area; Bruni *et al*., 2002). Interestingly, in this model the switch from Mg-HCO_3 to Ca-OH waters is caused by precipitation of sepiolite. As a matter of fact, the serpentinites surrounding modern alkaline springs of the Voltri 'massif' are locally pervaded by thin veins of sepiolite, whose formation has been put in relation with the alkaline fluids themselves (Schwarzenbach *et al*., 2013). A similar mechanism, involving the low-temperature interaction of fluids with serpentines and peridotites, could be also envisaged for the local precipitation of the studied sepiolite, as well as the generation of the related hydrocarbons.

The association of sepiolite with abiotic aliphatic hydrocarbons has been reported only once by Giustetto *et al*., 2014), who proved this coupling to favour defibrillation of the sepiolite crystals, with a consequent increase in the interfibre porosity (open texture) and modification of the fibre morphology, enhancing its length vs. thickness ratio from 'high' to 'very high'. Obviously, a similar phenomenology can be hypothesized also for the Sassello sepiolite. The thinner and exceptionally long fibrils (rods and/or laths; García-Romero and Suárez, 2013) may thus become potentially dangerous for human health, if aero-dispersed and inhaled.

4. Conclusions

An asbestiform sepiolite occurrence – in cm-thick veins within the serpentinites of the Voltri Unit cropping out near Sassello – was studied, in order to characterize its morphological habit and structural features and thus evaluate its possible hazard for human health. This sepiolite is formed by pluricentimetric flexible fibres that, when observed with SEM, appear as bundles of thinner intertwined fibrils (length > 100 μm). FT-IR analyses show the presence of moderate amounts of aliphatic hydrocarbons (yet to be thoroughly identified) coupled to these fibres – an atypical association reported only once in the literature (Giustetto *et al*., 2014).

These long and thin fibrils (or laths) might cause this sepiolite specimen to be potentially dangerous for human health, due to their latent carcinogenic risk if aero-dispersed and breathed in high doses. Besides, the contextual presence of aliphatic hydrocarbons may alter the fibrils surface reactivity, altering their capability of interacting with the pulmonary epithelium. The toxicity of occasional inhalation, skin absorption or ingestion of aliphatic hydrocarbons has also been acknowledged (Farinha *et al*., 2011). In the most recent report of the International Agency for Research on Cancer (IARC, 1997), an "inadequate evidence in humans for the carcinogenicity of sepiolite" is assessed. However, a "limited evidence in experimental animals for the carcinogenicity of long fibres" (> 5 μm) was suggested. Sepiolite fibres were included by IARC in "Group 3", implying that further investigations are needed to evaluate their effective noxiousness (IARC, 2012). Fortunately, the risk of inhaling high doses of the Sassello sepiolite fibres was averted by reclaiming the outcrop where the sample had been found.

Impending studies will be aimed at evaluating and comparing the potential carcinogenic risk of this and other similar sepiolite occurrences, in view of the peculiar association with the organic compounds that might affect their reactivity towards living cells and/or tissues.

Acknowledgements

The authors are deeply indebted to Cesare Atzori, for his help in collecting TGA data, and to Emanuele Costa and Elena Belluso, for their contributions in collecting and interpreting SEM-EDS data. Roberto Compagnoni is thanked for his help in interpreting analyses on thin sections at the polarizing microscope. Special thanks go to Carlotta Giacobbe and Rossella Arletti, for their support in collecting synchrotron XRPD diffraction patterns**.** We would like to thank the reviewers of this paper (Fabio Carmelo Manuella and an anonymous), who helped – with their hints and comments – to significantly improve the scientific weight of the manuscript.

Special thanks go to Marco Ciriotti, Giuseppe Pipino and Roberto Cabella, without whom this work could not have been.

References

Ahlrichs, J. L., Serna, C., Serratosa, J. M. (1975) Structural hydroxyls in sepiolite. *Clays Clay Miner*., 23, 119-124.

Àlvarez, A., Santarén, J., Esteban-Cubillo, A. and Aparaicio P. (2011) Current industrial applications of palygorskite and sepiolite. Pp. 281-298 in: *Developments in palygorskite-sepiolite research, a new outlook on these nanomaterials* (E. Galan and A. Singer, editors). Elsevier B.V.

Artioli, G. and Galli, E. (1994) The crystal structures of orthorhombic and monoclinic palygorskite. *Material Science Forum*, **166**, 647-652.

Bach, W., Banerjee, N.R., Dick, H.J.B. and Baker, E.T. (2002) Discovery of ancient and active hydrothermal systems along the ultra- slow spreading Southwest Indian Ridge 10°–16°E. *Geochemistry, Geophysics, Geosystems*, **3(7)**, 1-14.

Bailey, S.W., Alietti, A., Brindley, G.W., Formosa, M.L.L., Jasmund, K., Konta, J., Mackenzie, R.C., Nagasawa, K., Rausell-Colom, R.A. and Zvyagin, B.B. (1980) Summary of recommendations of AIPEA nomenclature committee. *Clays and Clay Minerals*, **28(1)**, 73-78.

Bellman, B., Muhle, H. and Ernst, H. (1997) Investigations on health-related properties of two sepiolite samples. *Environmental Health Perspectives*, **105(5)**, 1049-1052.

Belluso, E., Compagnoni, R. and Ferraris, G. (1995) Occurrence of asbestiform minerals in the serpentinites of the Piemonte Zone, Western Alps. Pp. 57-64 in: *Giornata di studio in ricordo del Prof. Stefano Zucchetti, Politecnico di Torino* (Politecnico di Torino, editor).

Belluso, E. and Sandrone, R. (1989) Occurrence of sepiolite in the marbles of the Dora Maira Massif (Italian Western Alps). *Mineralogica et Petrographica Acta*, **32**, 67-74.

Birsoy, R. (2002) Formation of sepiolite-palygorskite and related minerals from solution. *Clays and Clay Minerals*, **50(6)**, 736-745.

Bonatti, E., Craig Simmons, E., Breger, D., Hamlyn, P.R. and Lawrence, J. (1983) Ultramafic rock/seawater interaction in the oceanic crust: Mg-silicate (sepiolite) deposit from the Indian Ocean floor. *Earth and Planetary Science Letters*, **62**(2), 229-238.

Boschetti, T., Etiope, G. and Toscani, L. (2013) Abiothic methane in the hyperalkaline springs of Genova, Italy. *Procedia Earth and Planetary Science*, **7**, 248-251.

Boulart, C., Chavagnac, V., Monnin, C., Delacour, A., Ceuleneer, G. and Hoareau, G. (2012) Differences in gas venting from ultramafic-hosted warm springs: the example of Oman and Voltri ophiolites. *Ofioliti*, **38 (2)**, 143-156.

Brauner, K. and Preisinger, A. (1956) Structur und Enstehung des sepioliths. *Tschermaks Mineralogische und Petrographische Mitteilungen*, **6**, 1-2.

Brell, J.M., Doval, M. and Caramés, M. (1985) Clay mineral distribution in the evaporitic Miocene sediments of the Tajo Basin, Spain. *Mineralogica et Petrographica Acta*, **29-A**, 267-276.

Brindley, G.W. (1959) X-ray and electron diffraction data for sepiolite. *American Mineralogist*, **44**, 495-500.

Bruni, J., Canepa, M., Chiodini, G., Cioni, R., Cipolli, F., Longinelli, A., Marini, L., Ottonello, G. and Vetuschi Zuccolini, M. (2002) Irreversible water-rock mass transfer accompanying the generation of the neutral, Mg-HCO3 and high-pH, Ca-OH spring waters of the Genoa province, Italy. *Applied Geochemistry*, **17**, 455-474.

Bukas, V.J., Tsampodimou, M., Gionis, V. and Chryssikos, G.D. (2013) Synchronous ATR infrared and NIR spectroscopy investigation of sepiolite upon drying. *Vibrational Spectroscopy*, **68**, 51-60.

Cannings, F.R. (1968) An Infrared study of hydroxyl groups in sepiolite. *Journal of Physical Chemistry*, **72**, 1072-1074.

Capponi, G., Crispini, L., Piazza, M. and Amandola, L. (2001) Field constraints to the Mid-Tertiary kinematics of the Ligurian Alps. *Ofioliti*, **26 (2b)**, 409-416.

Capponi, G. and Crispini, L. (2002) Structural and metamorphic signature of Alpine tectonics in the Voltri Massif (Ligurian Alps, North Western Italy). *Eclogae Geologicae Helvetiae*, **95**, 31-42.

Capponi, G. and Crispini, L. (2008) Carta Geologica d'Italia alla scala 1.50.000 e Note Illustrative. Foglio 213-230 (Genova). APAT, Roma.

Capponi, G., Crispini, L. and Federico, L., (eds) (2013) Carta Geologica d'Italia alla scala 1.50.000 e Note Illustrative. Foglio 212 (Spigno Monferrato), parte ligure. Regione Liguria - Dipartimento Ambiente, Genova.

Capponi, G., Crispini, L., Federico, L. and Malatesta, C. (2016) Geology of the Eastern Ligurian Alps: a review of the tectonic units. *Italian Journal of Geosciences*, **135 (1)**, 157-169.

Chahi, A., Fritz, B., Duplay, J., Weber, F. and Lucas, J. (1997) Textural transition and genetic relationship between precursor stevensite and sepiolite in lacustrine sediments (Jbel Rhassoul, Morocco). *Clays and Clay Minerals*, **45**(3), 378-389.

Charlou, J.L., Fouquet, Y., Bougault, H., Donval, J.P., Etoubleau, J., Jean-Baptiste, P., Dapoigny, A., Appriou, P. and Rona, P.A. (1998) Intense CH_4 plumes generated by serpentinization of ultramafic rocks at the intersection of the 15°20′N fracture zone and the Mid-Atlantic Ridge. *Geochimica et Cosmochimica Acta*, **62 (13)**, 2323–2333.

Charlou, J.L., Donval, J.P., Fouquet, Y., Jean-Baptiste, P. and Holm, N. (2002) Geochemistry of high H_2 and CH_4 vent fluids issuing from ultramafic rocks at the Rainbow hydrothermal field, 36°14′N, MAR. *Chemical Geology*, **191**, 345–359.

Chavagnac., V., Monnin, C., Ceuleneer, G., Boulart, C. and Hoareau, G. (2013) Characterization of hyperalkaline fluids produced by low-temperature serpentinization of mantle peridotites in the Oman and Ligurian ophiolites. *Geochemistry, Geophysics, Geosystems*, **14 (7)**, 2496-2522.

Chiari, G., Giustetto, R. and Ricchiardi, G. (2003) Crystal structure refinements of palygorskite and Maya Blue from molecular modeling and powder synchrotron diffraction. *European Journal of Mineralogy*, **15**, 21–33.

Chiesa, S., Cortesogno, L., Forcella, F., Galli, M., Messiga, B., Pasquaré, G., Pedemonte, G.M., Piccardo, G.B. and Rossi, P.M. (1975) Assetto strutturale ed interpretazione geodinamica del gruppo di Voltri. *Bollettino della Società Geologica Italiana.*, **94**, 555-581.

Ciliberto, E., Crisafulli, C., Manuella, F.C., Samperi, F., Scirè, S., Scribano, V., Viccaro, M. and Viscuso E. (2009) Aliphatic hydrocarbons in metasomatized gabbroic xenoliths from Hyblean diametres (Sicily): genesis in a serpentinite hydrothermal system. *Chemical Geology*, **258**, 258-268.

Cipolli, F., Gambardella, B., Marini, L., Ottonello, G. and Vetuschi Zuccolini, M. (2004) Geochemistry of high-pH waters from serpentinites of the Gruppo di Voltri (Genova, Italy) and reaction path modeling of CO_2 sequestration in serpentinite aquifers. *Applied geochemistry*, **19**, 787-802.

Cuevas, J, Leguey, S. and Ruiz, A.I. (2012) Evidence for the biogenic origin of sepiolite. Pp. 219-238 in: *Developments in palygorskite-sepiolite research, a new outlook on these nanomaterials* (E. Galan E. and A. Singer, editors). Elsevier B.V.

d'Atri, A., Irace, A., Piana, F., Tallone, S., Varrone, D., Bellino, L., Fioraso, G., Cadoppi, P., Fusetti, E., Morelli, M., Lanteri, L. Paro, L., Piccini, C., Trenkwalder, S. and Violanti, D. (2016) Carta Geologica d'Italia alla scala 1.50.000 e Note Illustrative. Foglio 194 (Acqui Terme). ISPRA, Roma.

d'Atri, A., Irace, A., Piana, F., Tallone, S., Bodrato, G. and Roz Gastaldi, M. (1997) Tettonica oligo-miocenica nell'Alto Monferrato (Bacino Terziario Piemontese) e nel settore nord-occidentale del Gruppo di Voltri (Acqui Terme-Cassinelle, AL). *Atti Ticinensi di Scienze della Terra, Serie Speciale*, **5**, 85-100.

del Buey, P., Cabastrero, O., Arroyo, X. and Sanz-Montero, M.E. (2018) Microbially induced palygorskite-sepiolite authigenesis in modern hypersaline lakes (Central Spain). *Applied Clay Science*, **160**, 9-21.

Dollase, W.A. (1986) Correction of intensities for preferred orientation in powder diffractometry: application of the March model. *Journal of Applied Crystallography*, **19**, 267-272.

Dos Anjos, C.W.D., Meunier, A., Guimaraès, E.M. and El Albani, A. (2010) Saponite-rich black shales and nontronite beds of the Permian Irati Formation: sediment sources and thermal metamorphism (Parana´ Basin, Brazil). *Clays and Clay Minerals*, **58**, 606-626.

Ehlmann, A.J., Sand, L.B. and Regis, A.J. (1962) Occurrences of sepiolite in Utah and Nevada. *Economic Geology*, **57 (7)**, 1085-1094.

Etiope, G. and Sherwood Lollar, B. (2013) Abiotic methane on Earth. *Reviews of Geophys*ics, **51**, 276-299.

Eugster, H.P. and Hardie, L.A. (1975) Sedimentation in an ancient playa-lake complex: the Wilkins Peak member of the Green River Formation of Wyoming. *Bulletin of the Geological Society of America*, **86**, 319-334.

Farinha, A., Assunção, J. and Vinhas, J. (2011) Renal toxicity of inhaled aliphatic hydrocarbons: a case report of chronic interstitial nephropathy. *Port J. Nephrol. Hypert*, **25(1)**, 43-46.

Federico, L., Crispini, L., Dabove, G.M., Piazza, M. and Capponi, G. (2016) Stratigraphic vs structural contacts in a late orogenic basin: the case of the Tertiary Piedmont Basin in the Sassello area (Ligurian Alps, Italy). *Journal of Maps*, **12 (5)**, 959-967.

Ferraris, G., Makovicky, E. and Merlino, S. (2008) in: *Crystallography of modular materials*. Oxford, IUCr. Oxford University Press.

Finger, L.W., Cox, D.E. and Jephcoat, A.P. (1994) A correction for powder diffraction peak asymmetry due to axial convergence. *Journal of Applied Crystallography*, **27**, 892-900.

Frost, R.L., Cash, G.A. and Kloprogge, J.T. (1998) 'Rocky Mountain leather', sepiolite and attapulgite-an infrared emission spectroscopic study. *Vibrational Spectroscopy*, **16**, 173-184.

Frost, R.L. and Ding, Z. (2003) Controlled rate thermal analysis and differential scanning calorimetry of sepiolites and palygorskites. *Thermochimica Acta*, **397(1-2)**, 119-128.

Frost, R.L., Kristòf, J. and Horvàth, E. (2009) Controlled rate thermal analysis of sepiolite. *Journal of Thermal Analysis and Calorimetry*, **98(3)**, 749-755.

Frost, R.L., Locos, O.B., Ruan, H. and Kloprogge, J.T. (2001) Near-infrared spectroscopic study of sepiolites and palygorskites. *Vibrational Spectroscopy*, **27**, 1-13.

Galán, E. and Pozo, M. (2011) Palygorskite and sepiolite deposits in continental environments. Description, genetic patterns and sedimentary settings. Pp. 131-135 in: *Developments in palygorskite-*

sepiolite research, a new outlook on these nanomaterials (E. Galan E. and A. Singer, editors). Elsevier B.V.

García-Rivas, J., Sánchez del Río, M., García-Romero, E. and Suárez, M. (2017) An insight in the structure of a palygorskite from Palygorskaja: Some questions on the standard model. *Applied Clay Science*, **148**, 39-47.

García-Romero, E. and Suarez, M. (2010) On the chemical composition of sepiolite and palygorskite. *Clays and Clay Minerals*, **58**, 1-20.

García-Romero, E. and Suárez, M. (2013) Sepiolite-palygorskite: textural study and genetic considerations. *Applied Clay Science*, **86**, 129-144.

García-Romero, E. and Suárez, M. (2014) Sepiolite-palygorskite polysomatic series: Oriented aggregation as a crystal growth mechanism in natural environments. *American Mineralogist*, **99** (8-9), 1653-1661.

Giustetto, R. and Chiari, G. (2004) Crystal structure refinement of palygorskite from neutron powder diffraction. *European Journal of Mineralogy*, **16**, 521-532.

Giustetto, R. and Compagnoni, R. (2011) An unusual occurrence of palygorskite from Montestrutto, Sesia-Lanzo Zone, internal Western Alps (Italy). *Clay Minerals*, **46**, 371-385.

Giustetto, R., Levy, D., Wahyudi, O., Ricchiardi, G. and Vitillo, J.G. (2011a) Crystal structure refinement of a sepiolite/indigo Maya Blue pigment using molecular modelling and synchrotron diffraction. *European Journal of Mineralogy*, **23**, 449-466.

Giustetto, R., Seenivasan, K., Bonino, F., Ricchiardi, G., Bordiga, S., Chierotti, M.R. and Gobetto, R. (2011b) Host/guest interactions in a sepiolite-based Maya Blue pigment: a spectroscopic study. *Journal of Physical Chemistry C*, **115**, 16764-16776.

Giustetto, R., Wahyudi, O., Corazzari, I. and Turci, F. (2011c) Chemical stability and dehydration behaviour of a sepiolite/indigo Maya Blue pigment. *Applied Clay Science*, **52**, 41-50.

Giustetto, R., Seenivasan, K., Belluso, E. (2014). Asbestiform sepiolite coated by aliphatic hydrocarbons from Perletoa, Aosta Valley Region (Western Alps, Italy): characterization, genesis and possible hazards. *Mineralogical Magazine*, **78(4)**, 919-940.

Grim, R.E. (1968) *Clay Mineralogy*. McGraw-Hill, New York, 384 pp.

Guggenheim, S. and Krekeler, M.P.S. (2011) The structure and microtextures of the palygorskite-sepiolite Group minerals. Pp. 15-16 in: *Developments in palygorskite-sepiolite research, a new outlook on these nanomaterials* (E. Galan and A. Singer, editors). Elsevier B.V.

Hayashi, H., Otsuka, R. and Imai, N. (1969) Infrared study of sepiolite and palygorskite on heating. *American Mineralogist*, **54**, 1613-1624.

Hodeau, J.L., Bordet, P., Anne, M., Prat, A., Fitch, A.N., Dooryhee, E., Vaughan, G. and Freund, A. (1998) Nine crystal multi-analyser stage for high-resolution powder diffraction between 6 and 40 keV. *Proceedings of SPIE*, **3448**, 353.

Imai N. and Otsuka, R. (2000) Sepiolite and palygorskite in Japan. Pp. 211-232 in: *Palygorskite – sepiolite: occurrences, genesis and uses* (A. Singer and E. Galan, eds). *Developments in Sedimentology*, **37**.

International Agency for Research on Cancer, World Health Organization (1997) Sepiolite. Pp. 267-282 in: *IARC Monographs on the evaluation of carcinogenic risks to humans; Silica, some silicates, coal dust and para-aramid fibrils*. **68**, IARC Press.

International Agency for Research on Cancer, World Health Organization (2012). Arsenic, metals, fibres, and dusts. Pp. 501 in: *Monographs on the evaluation of carcinogenic risks to humans; A review of human carcinogens.* **100 C**, IARC Press.

Jeffrey, G.A. (1997) *An introduction to hydrogen bonding*, Oxford University Press. pp?

Jones, B.F. and Galan, E. (1988) Palygorkite and sepiolite. Pp. 631-674 in: *Hydrous Phyllosilicates* (S.W. Bailey, ed), Reviews in Mineralogy, **19**. Mineralogical Society of America, Washington.

Jung, S.M. and Grange, P. (2004) Characterization of the surface hydroxyl properties of sepiolite and $Ti(OH)_4$ and investigation of new properties generated over physical mixture of $Ti(OH)_4$-sepiolite. *Applied Surface Science*, **221**, 167-177.

Karakaya, M.C., Karakaya, N. and Temel, A. (2011) Mineralogical and geochemical characteristics and genesis of the sepiolite deposits at Polatli basin (Ankara, Turkey). *Clays and Clay Minerals*, **59(3)**, 286–314.

Konn, C., Charlou, J.L., Donval, J.P., Holm, N.G., Dehairs, F. and Bouillon, S. (2009) Hydrocarbons and oxidized organic compounds in hydrothermal fluids from Rainbow and Lost City ultramafic-hosted vents. *Chemical Geology*, **258**, 299-314.

Kovács-Pálffy, P., Kónya, P., Kalmár, J., Fehér, B. and Földvári, M. (2016) A hydrothermal sepiolite occurrence at Măgureni Hill, Preluca Veche (Maramureş County, Romania). *Földtani Közlöny*, **146 (4)**, 321-334.

Krekeler, M.P.S. and Guggenheim, S. (2009) Defects in microstructure in palygorskite-sepiolite minerals: a transmission electron microscopy (TEM) study. *Applied Clay Science*, **39**, 98-105.

Larson, A.C. and Von Dreele, R.B. (2007) *GSAS – General Structure Analysis System*. Los Alamos National Laboratory Report No. LAUR 86-748.

Leguey, S., Ruiz de Leòn, D., Ruiz, A.I. and Cuevas, J. (2010) The role of biomineralization in the origin of sepiolite and dolomite. *American Journal of Science*, **310**, 165-193.

Lòpez-Galindo, A., Viseras, C., Aguzzi, C. and Cerezo, P. (2011) Pharmaceutical and cosmetic uses of fibrous clays. Pp. 299-324 in: *Developments in palygorskite-sepiolite research, a new outlook on these nanomaterials* (E. Galan and A. Singer, editors). Elsevier B.V.

Macdonald, A.H. and Fyfe, W.S. (1985) Rate of serpentinization in seafloor environments. *Tectonophysics*, **116**, 123-135.

Manuella, F.C., Carbone, S. and Barreca, G. (2012) Origin of saponite-rich clays in a fossil serpentinite-hosted hydrothermal system in the crustal basement of the Hyblean plateau (Sicily, Italy). *Clays and Clay Minerals*, **60(1)**, 18-31.

Marcaillou, C., Muñoz, M., Vidal, O., Parra, T. and Harfouche, M. (2011) Mineralogical evidence for H_2 degassing during serpentinization at 300ºC/300 bar. *Earth and Planetary Science Letters*, **303**, 281-290.

March, A. (1932) Mathematische Theorie der Regelung nach der Korngestalt bei affiner Deformation. *Zeitschrift für Kristallographie*, **81**, 285-297.

Mayayo, M.J., Torres-Ruiz, J., Gonzalez-Lopez, J.M., Lopez-Galindo, A. and Bauluz, B. (1998) Mineralogical and Chemical characterization of the sepiolite/Mg-smectite deposit at Mara (Calatayud basin, Spain). *European Journal of Mineralogy*, **10**, 367-383.

Mendelovici, E. (1973) Infrared study of attapulgite and HCl treated attapulgite. *Clays and Clay Minerals*, **21**, 115-119.

Mendelovici, E. and Portillo, D.C. (1976) Organic derivatives of attapulgite-I. Infrared spectroscopy and X-ray diffraction studies. *Clays and Clay Minerals*, **24**, 177-182.

Messiga, B. and Scambelluri, M. (1991) Retrograde P-T-t path for the Voltri Massif eclogites (Ligurian Alps, Italy): some tectonic implications. *J. Metam. Geol*., 9(19, 93-109.

Mifsud, A., Garcia, I. and Corma, A. (1987) Thermal stability and textural properties of exchanged sepiolites. Pp. 392-394 in: *Proceedings Euroclay '87*. Sociedad Espanola de Arcilla, Sevilla.

Molli, G., Crispini, L., Malusà, M. G., Mosca, P., Piana, F. and Federico, L. (2010) Geology of the Western Alps-Northern Apennine junction area: a regional review. *Journal of the Virtual Explorer*, **36**, 3.

Nagata, H., Shimoda, S. and Sudo, T. (1974) On dehydration of bound water in sepiolite. *Clays and Clay Minerals*, **22**, 285-293.

O'Driscoll, M. (1992) European cat litter. Absorbing market growth. *Industrial Minerals*, **299**, 46-65.

Ordoñez, S., Calvo, J.P., Garcìa del Cura, M.A., Alonso Zarza, A.M. and Hoyos, M. (1991) Sedimentology of sodium sulphate deposits and special clays from the Tertiary Madrid Basin (Spain). In: Anadòn, P., Cabrera, L.I., Keiths, K. (Eds.), *Lacustrine Facies Analysis, Special Publications of*

the International Association of Sedimentologists, vol. **13**, Blackwell Scientific Publications, Oxford, pp. 39-55.

Ovarlez, S., Giulieri, F., Chaze, A.M., Delamare, F., Raya, J. and Hirschinger J. (2009) The incorporation of indigo molecules in sepiolite tunnels. *Chemistry A European Journal*, **15**, 11326-11332.

Ovarlez, S., Giulieri, F., Delamare, F., Sbirrazzuoli, N. and Chaze, A.M. (2011) Indigo-sepiolite nanohybrids: temperature-dependent synthesis of two complexes and comparison with indigo-palygorskite systems. *Microporous and Mesoporous Materials*, **142**, 371-380.

Piana, F., d'Atri, A. and Orione, P. (1997) The Visone Formation: a marker of the Early Miocene tectonics in the Alto Monferrato domain (Tertiary Piemonte Basin, NW Italy). *Memorie di Scienze Geologiche*, **49**, 145-162.

Piana, F., Fioraso, G., Irace, A., Mosca, P., d'Atri, A., Barale, L., Falletti, P., Monegato, G., Morelli, M., Tallone, S. and Vigna, G.B. (2017) Geology of Piemonte region (NW Italy, Alps-Apennines interference zone). *Journal of Maps*, **13(2)**, 395-405.

Piana, F., Tallone, S., Cavagna, S. and Conti, A. (2006) Thrusting and faulting in metamorphic and sedimentary units of Ligurian Alps: an example of integrated field work and geochemical analyses. *International Journal of Earth Sciences*, **95**, 413-430.

Piccardo, G.B. (1984) Le ofioliti del gruppo di Voltri, Alpi Liguri: caratteri primari ed interpretazione geodinamica. *Memorie della Società Geologica Italiana*, **28**, 95-114.

Post, J.E., Bish, D.L. and Heaney P.J. (2007) Synchrotron powder X-ray diffraction study of the structure and dehydration behavior of sepiolite. *American Mineralogist*, **92**, 91-97.

Post, J.E. and Heaney, P.J. (2008) Synchrotron powder diffraction study of the structure and dehydration behavior of palygorskite. *American Mineralogist*, **93**, 667-675.

Pott, F., Bellman, B., Muhle, H., Rödelsperger, K., Rippe, R.M., Roller, M. and Rosenbruch, M. (1990) Intraperitoneal injection studies for the evaluation of the carcinogenicity of fibrous phyllosilicates. Pp. 319-329 in: *Health Related Effects of Phyllosilicates* (J. Bignon, editor). North Atlantic Treaty Organization Advanced Study Institute Series, Vol. G21, Ecological Sciences, Berlin West, Springer-Verlag.

Pott, F., Roller, M., Rippe, R.M., Germann, P.G. and Bellman, B. (1991) Tumors by the intraperitoneal and intrapleural routes and their significance for the classification of mineral fibres. Pp. 547-565 in: *Mechanisms in Fibre Carcinogenesis* (R.C. Brown, J.A. Hoskins and N.F. Johnson, editors). New York/London Plenum Press.

Preisinger, A. (1959) X-ray study of the structure of sepiolite. *Clays and Clay Minerals*, **6**, 61-67.

Proskurowski, G., Lilley, M.D. and Seewald, J.S. (2008) Abiogenic hydrocarbon production at Lost City hydrothermal field. *Science*, **319**, 604-607.

Ruiz, R., del Moral, J.C., Pesquera, C., Benito, I. and González, F. (1996) Reversible folding in sepiolite: study by thermal and textural analysis. *Thermochimica Acta*, **279**, 103–110.

Sanchez del Rio, M., Garcia-Romero, E., Suarez, M., da Silva, I., Fuentes Montero, L. and Martinez-Criado, G. (2011) Variability in sepiolite: Diffraction studies. *American Mineralogist*, **96**, 1443-1454.

Schwarzenbach, E.M., Lang S.Q., Früh-Green, G.L., Lilley M.D., Bernasconi, S.M. and Méhay, S. (2013) Sources and cycling of carbon in continental, serpentine-hosted alkaline springs in the Voltri Massif, Italy. *Lithos*, **177**, 226-244.

Sciré, S., Ciliberto, E., Crisafulli, C., Scribano, V., Bellatreccia, F. and Della Ventura, G. (2011) Asphaltene-bearing mantle xenoliths from Hyblean diatremes, Sicily. *Lithos*, **125**, 956-968.

Serna, C., Ahlrichs, J.L. and Serratosa, J.M. (1975) Folding in sepiolite crystals. *Clays and Clay Minerals*, **23**, 452-457.

Solebello, L. (2009) Fibrous sepiolite use as an asbestos substitute: analytical basics. *Microscopy Today*, **15**, 18-19.

Spagnolo, C., Crispini, L. and Capponi, G. (2004) Late orogenic structural evolution in the Ligurian Alps: case history from the Voltri Group. *Ofioliti*, **29(2)**, 255.

Spagnolo, C., Crispini, L. and Capponi, G. (2007) Late structural evolution in an accretionary wedge: insights from the Voltri Massif (ligurian Alps, Italy). *Geodinamica Acta*, **20 (1-2)**, 21-35.

Suárez, M. and García-Romero, E. (2011) Advances in the Crystal Chemistry of Sepiolite and Palygorskite. Pp. 33-65 in: *Developments in Palygorskite-Sepiolite Research, a new outlook on these nanomaterials* (E. Galan and A. Singer, editors). Elsevier B.V.

Suárez, M. and García-Romero, E. (2012) Variability of the surface properties of sepiolite. *Applied Clay Science*, **67-68**, 72-82.

Taran, Y.A., Kliger, G.A. and Sevastianov, V.S. (2007) Carbon isotope effects in the open system Fischer–Tropsch synthesis. *Geochimica et Cosmochimica Acta*, **71**, 4474–4487.

Thompson, P., Cox, D.E. and Hastings, J.B. (1987) Rietveld refinement of Debye-Scherrer synchrotron data from Al_2O_3. *Journal of Applied Crystallography*, **20**, 79–83.

Toby, B.H. (2001) EXPGUI, a graphical user interface for GSAS. *Journal of Applied Crystallography*, **34**, 210-213.

Trauth, N. (1977) Argiles évaporitiques dans les sédimentation carbonatée et épicontinentale tertiaire, Bassin de Paris, de Mormoiron et de Salìnelles (France), Ibel Ghassoul (Maroc). *Mémoires de Sciences Géologiques*, **49**, pp. 195.

Ugliengo, P., Viterbo, D. and Chiari, G. (1993) MOLDRAW: molecular graphics on a personal computer. *Kristallographie*, **207**, 9.

Velde, B. (1985) Clay minerals: a physic-chemical explanation of their occurrences. In: *Developments in Sedimentology*, **40**, Elsevier, Nueva York, pp. 187-198.

Vitale Brovarone, A., Martinez, I., Elmaleh, A., Compagnoni, R., Chaduteau, C., Ferraris, C. and Esteve, I. (2017) Massive production of abiotic methane during subduction evidenced in metamorphosed ophicarbonates from the Italian Alps. *Nature Communications*, **8**, 14134.

Weaver, C.E. (1984) Origin and geologic implications of the palygorskite deposits of SE United States. In: Singer, A., Galàn, E. (Eds.), Palygorskite-Sepiolite: Occurrences, Genesis and Uses. *Developments in Sedimentology*, **37**, Elsevier, Amsterdam, pp. 39-58.

Weir, M.R., Kuang, W., Facey, G.A. and Detellier, C. (2002) Solid-state nuclear magnetic resonance study of sepiolite and partially dehydrated sepiolite. *Clays and Clay Minerals*, **50**, 240–247.

Yalçin, H. and Bozkaya, Ö. (2004) Ultramafic-rock-hosted vein sepiolite occurrences in the Ankara ophiolitic Mélange, central Anatolia, Turkey. *Clays and clay minerals*, **52 (2)**, 227-239.

Table Captions

Table 1. Chemical composition (weight % oxides and mean value) and cations number calculated on an anhydrous basis (32 oxygens) of the sepiolite specimen from the Deiva forest.

Table 2. TGA weight losses and related attributions for the Deiva forest sepiolite.

Table 3. FT-IR active vibrational modes and related attributions at different temperatures and vacuum conditions for the Deiva forest sepiolite and the associated aliphatic hydrocarbons.

Table 4. Crystal-chemical formula, space group, cell parameters and refinement data for the Deiva forest sepiolite.

Table 5. Refined fractional atomic coordinates, occupancy factors and isotropic displacement parameters for the Deiva forest sepiolite.

Tables

Oxides (wt%)	1	2	3	4	5	6	7	8	9	10	Average
SiO_2	56.34	58.35	57.58	57.92	57.86	57.02	57.77	58.43	58.83	58.83	57.8(8)
Fe_2O_3	4.98	5.41	5.54	5.36	5.27	5.23	5.21	5.55	5.50	5.28	5.3(2)
Al_2O_3	=	=	=	=	0.01	=	0.05	=	=	=	0.00(2)
MgO	20.15	20.63	20.56	20.84	20.98	20.38	20.63	20.59	20.96	21.23	20.7(3)
Σ	81.47	84.39	83.68	84.12	84.12	82.63	83.66	84.57	85.29	85.34	84(1)
Cations											
Si	12.15	12.16	12.12	12.12	12.10	12.14	12.14	12.15	12.14	12.12	12.13(2)
Fe^{3+}	0.81	0.85	0.88	0.84	0.83	0.84	0.82	0.87	0.85	0.82	0.84(2)
Al^{3+}	=	=	=	=	0.003	=	0.012	=	=	=	0.002(4)
Mg	6.48	6.41	6.45	6.50	6.54	6.47	6.46	6.39	6.45	6.52	6.47(5)
Σ	19.44	19.42	19.45	19.46	19.473	19.45	19.432	19.41	19.44	19.46	19.44(2)

Table 1

Temperature range (° C)	Weigth loss (%)	DSC event	Attribution and comments
25 – 120	≈ 8	endothermic (90° C)	Loss of physisorbed water and less severely bound zeolitic H_2O (tetra-hydrated sepiolite; SEP4H_2O)
120 – 310	≈ 4.5	endothermic (290° C)	Loss of residual zeolitic H_2O and 1st fraction of structural OH_2 (di-hydrated sepiolite; SEP2H_2O)
310 – 630	≈ 3.5	= endothermic (760° C)	Loss of 2nd fraction of structural OH_2 (anhydrous sepiolite)
630 – 790	≈ 2.5	endothermic (800° C) exothermic (820° C)	Loss of framework OH (dehydroxylation) and transformation to clinoenstatite (or an amorphous phase)
Total	18.5		

Table 2

Sepiolite			
Room *T* in He flux (time: 0 min)	**Room *T* in He flux** (time: 60 mins)	**Heated at 400° C in He flux**	**Attribution and comments**
Stretching region (2750 - 3750 cm^{-1})			
3246	=	=	ν(OH) of physisorbed water, gradually lost by evacuating at room *T* in He flux
3350	=	=	ν(OH) of zeolitic H_2O, gradually lost by evacuating at room *T* in He flux
≈ 3582	≈ 3582	3528	ν(OH) of structural OH_2;
		3597	ν(OH) of structural OH_2;
		3654	ν(OH) of structural OH_2; shifts might be due to H-bond and variations in the antisymmetric and symmetric ν(OH_2)
3680	3680	3673	ν(OH) of hydroxyl in O sheet; shift at 400°C accounts for intervened folding of the sepiolite structure
=	=	3688	H-H repulsion of framework hydroxyls (Mg-OH), due to the approaching of residual OH_2 dislocated by structural folding
=	3720	3736	ν(Si-OH); perturbation of superficial silanols; Si-OH liberation at the edge of the O ribbons due to structure folding
Bending region (1400 - 1800 cm^{-1})			
1658	=	=	δ(H_2O) of physisorbed/zeolitic H_2O, gradually lost by evacuating at room *T* in He flux
1620	1622	1620	δ(H_2O) of structural OH_2; intensity decay with *T* rise accounts for gradual OH_2 loss
	1614	=	
1209	1192	=	Si-O stretch (???) Up-warded γ mode of residual zeolitic H_2O (???)
Aliphatic hydrocarbons			
Room *T* in He flux (time: 0 min)	**Room *T* in He flux** (time: 60 mins)	**Heated at 400° C in He flux**	**Attribution and comments**
Stretching region (2750 - 3750 cm^{-1})			
=	3207	=	ν(C-H); gradually decreases with *T* rise
=	2925	2925	ν(CH_2)
=	2858	2858	ν(CH_2)
Bending region (1400 - 1800 cm^{-1})			
1428	1428	1404	δ(C–H); gradually splits at 400° C
		1456	δ(CH_2) scissoring, δ(CH_3) asymmetric; gradually splits at 400° C

Table 3

Structural formula	$Si_{24}Mg_{16}O_{92.36}$
Space group (H-M)	*Pncn*
a (Å)	13.4577(5)
b "	27.0138(7)
c "	5.28083(14)
V (Å^3)	1919.82(10)
$\Delta\rho_{min}$, $\Delta\rho_{max}$ (e/Å^3)	-1.050; 0.870
R	0.0323
R_{wp}	0.0425
$R(F^2)$	0.1312
reduced χ^2	0.1455
GOF $[R_{wp}/R_{exp}]^2$	1.73

Table 4

Atom type	**Label**	***x***	***y***	***z***	**Fraction**	U_{iso}
Mg	Mg1	0	0.02855(19)	0.25	1.00	0.010(2)
Mg	Mg2	0	0.08699(22)	0.75	1.00	0.010(2)
Mg	Mg3	0	0.14285(21)	0.25	1.00	0.010(2)
Mg	Mg4	0	0.19995(21)	0.75	1.00	0.010(2)
O	O1	0.07510(35)	0.02823(29)	0.5809(18)	1.00	0.009(1)
OH	O2	0.0864(5)	0.08541(31)	0.0760(13)	1.00	0.009(1)
O	O3	0.0845(4)	0.14391(28)	0.5795(14)	1.00	0.009(1)
Si	Si1	0.19621(34)	0.02687(20)	0.5727(11)	1.00	0.0120(8)
Si	Si2	0.2056(4)	0.14140(19)	0.5821(11)	1.00	0.0120(8)
Si	Si3	0.2099(4)	0.19499(13)	0.0770(9)	1.00	0.0120(8)
O	O4	0.0889(4)	0.19816(29)	0.0794(14)	1.00	0.009(1)
O	O5	0.2422(5)	-0.0005(4)	0.3238(13)	1.00	0.009(1)
O	O6	0.2383(5)	0.08336(20)	0.5781(13)	1.00	0.009(1)
O	O7	0.2452(5)	0.1581(4)	0.3035(14)	1.00	0.009(1)
O	O8	0.2548(5)	0.1725(5)	0.8146(14)	1.00	0.009(1)
O	O9	0.25	0.25	0.1500(21)	1.00	0.009(1)
OH_2	SW10	0.0819(7)	0.25997(30)	0.6078(24)	0.92(2)	0.030(7)
H_2O	ZW11	0.5600(7)	-0.0810(5)	0.0385(21)	1.0	0.21(1)
H_2O	ZW12	=	=	=	0.0	=
H_2O	ZW13	0.5	0.0042(12)	0.25	0.69(4)	0.21(1)
H_2O	ZW14	0.5305(18)	0.1810(8)	0.5000(24)	0.78(2)	0.21(1)

Table 5

Figure captions

Figure 1. Geological scheme of the Beigua Geopark and its surroundings, at the boundary between Liguria and Piemonte regions (Alps-Apennines interference zone *sensu* Piana *et al*., 2017). The red rectangle indicates the position of the simplified geological map of Fig. 2.

Figure 2. Simplified geological map of the Deiva Forest-Sassello area (see position in Fig. 1), indicating the site of collection of the asbestiform sepiolite (star). Geological boundaries were redrawn from Federico *et al*. (2016); the D1 unconformity at the base of the Molare Formation is a regional unconformity of early Rupelian age which can be traced throughout the Tertiary Piemonte Basin (Piana *et al*., 2017, and references therein).

Figure 3. Macroscopic appearance of the sepiolite specimen from the Deiva forest: Notice how the fibrous habit is well evident even at the macroscopic scale, with exceptionally long fibres (up to several cm; see magnification in the upper right corner).

Figure 4. Secondary electron SEM images of the Deiva forest sepiolite: a) the anomalously long fibres (observed to the naked eye and with optical microscopy) are indeed made of bundles of thinner units (fibrils), running parallel and at times entangled; b) the true dimensions of these fibrils (length > 100 μm; thickness < 100 nm) become evident at higher magnifications.

Figure 5. Observed TGA/derivative weight and Differential Scanning Calorimetry (DSC) curves for the Deiva forest sepiolite.

Figure 6. FT-IR spectra collected on the Deiva forest sepiolite at room T in He flux for 1 hour, in order to favour the progressive loss of zeolitic H2O at a constant temperature; black and red spectra: 0 and 60 mins, respectively; grey curves: intermediate time. The inset reports a magnification, in the stretching region, of those bands related to aliphatic hydrocarbons.

Figure 7. FT-IR spectra collected on the Deiva forest sepiolite by gradually heating from room T (red) to 400 °C (black) under He flux, in order to appreciate consequent structural changes and further dehydration. Spectra measured at intermediate temperatures are reported in grey. The two insets report magnifications of the OH stretching at higher wavenumbers (on the left) and of hydrocarbon maxima in the bending region (on the right, highlighted with a square).

Figure 8. Crystal structure refinement with the Rietveld method of the Deiva forest sepiolite: observed (crosses) and calculated (solid line) diffraction patterns, background (grey dots) and related difference curve (lower line). Magnification (upper right corner) shows the diffraction patterns by excluding the stronger (110) reflection.

Figure 9. Refined crystal structure for the Deiva forest sepiolite (unit cell outlined as thin grey bars).

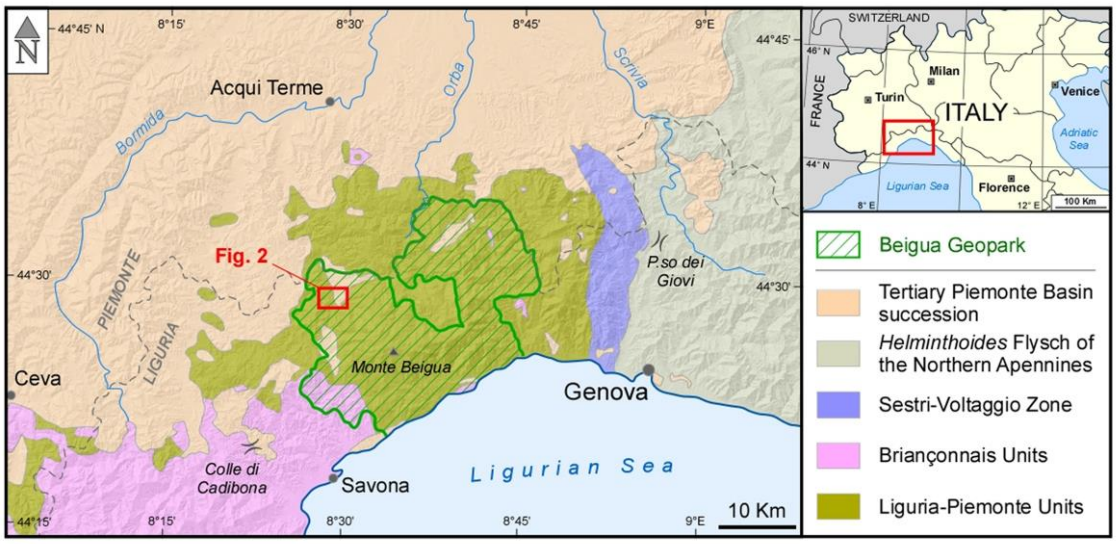
Acqui Terme
Bormida
Orba
Sorivia
Fig. 2
Monte Beigua
Ceva
Genova
Savona
Colle di Cadibona
P.so dei Giovi
PIEMONTE
LIGURIA
Ligurian Sea
10 Km
SWITZERLAND
FRANCE
Milan
Turin
Venice
ITALY
Adriatic Sea
Florence
Beigua Geopark
Tertiary Piemonte Basin succession
Helminthoides Flysch of the Northern Apennines
Sestri-Voltaggio Zone
Briançonnais Units
Liguria-Piemonte Units

Fig. 1

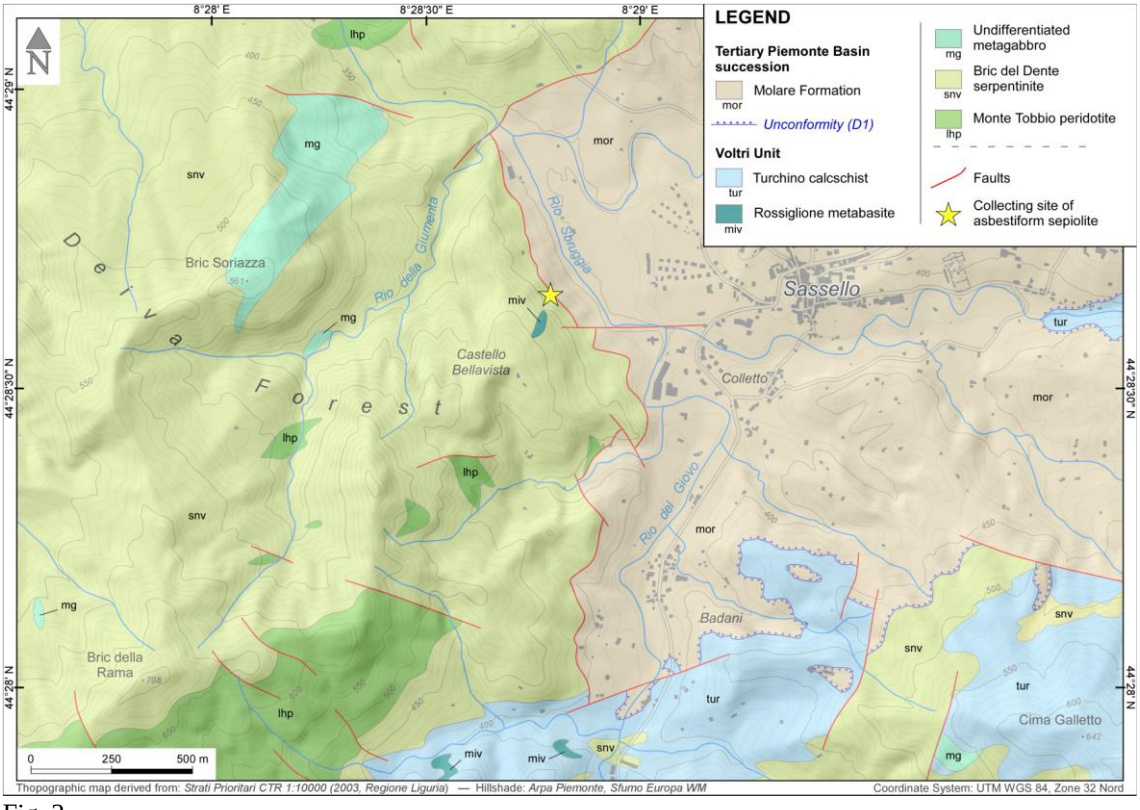
LEGEND
Tertiary Piemonte Basin succession
Molare Formation
Unconformity (D1)
Voltri Unit
Turchino calcschist
Rossiglione metabasite
Undifferentiated metagabbro
Bric del Dente serpentinite
Monte Tobbio peridotite
Faults
Collecting site of asbestiform sepiolite
Bric Soriazza
Rio della Giumenta
Rio Sbruggia
Sassello
Castello Bellavista
Colletto
Rio del Giovo
Badani
Bric della Rama
Cima Galletto
Deiva Forest
0 250 500 m
Thopographic map derived from: Strati Prioritari CTR 1:10000 (2003, Regione Liguria) — Hillshade: Arpa Piemonte, Sfumo Europa WM
Coordinate System: UTM WGS 84, Zone 32 Nord

Fig. 2

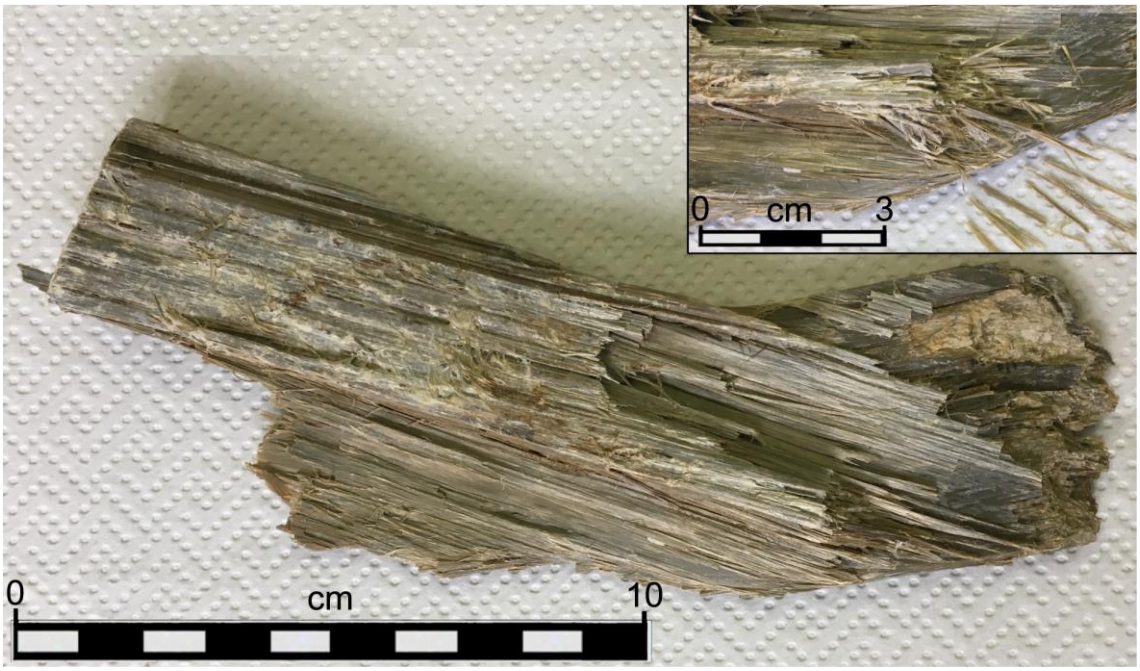
0
cm
3
0
cm
10

Fig. 3

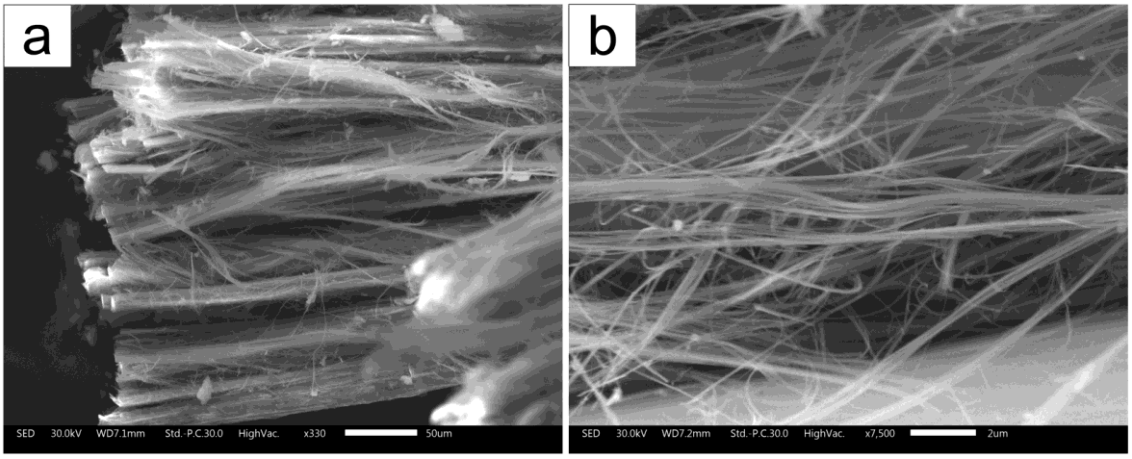
a
b
SED 30.0kV WD7.1mm Std.-P.C.30.0 HighVac. x330 50um
SED 30.0kV WD7.2mm Std.-P.C.30.0 HighVac. x7,500 2um

Fig. 4

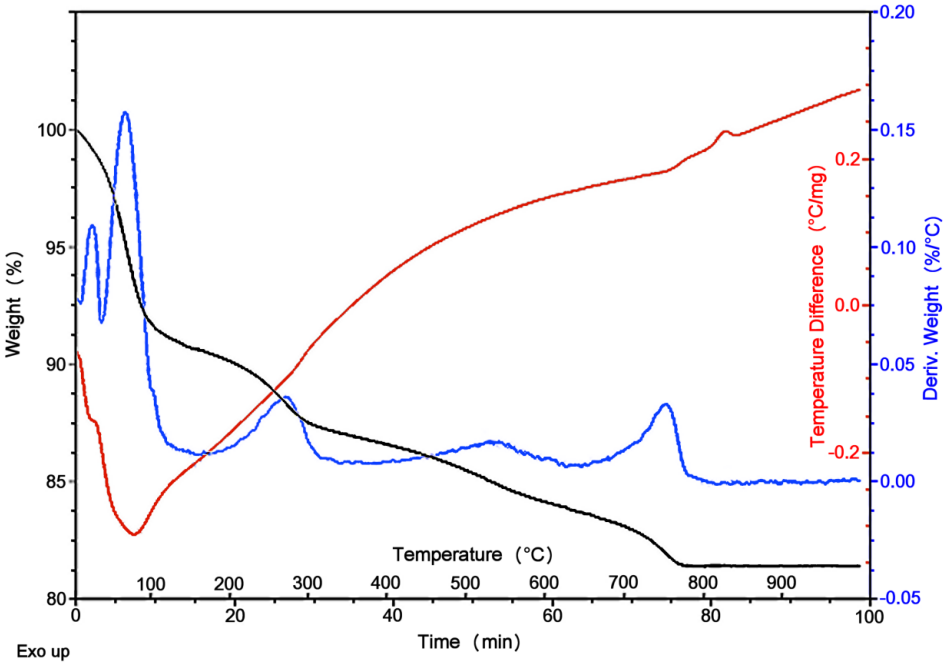
Weight (%)
Temperature Difference (°C/mg)
Deriv. Weight (%/°C)
Temperature (°C)
Time (min)
Exo up

Fig. 5

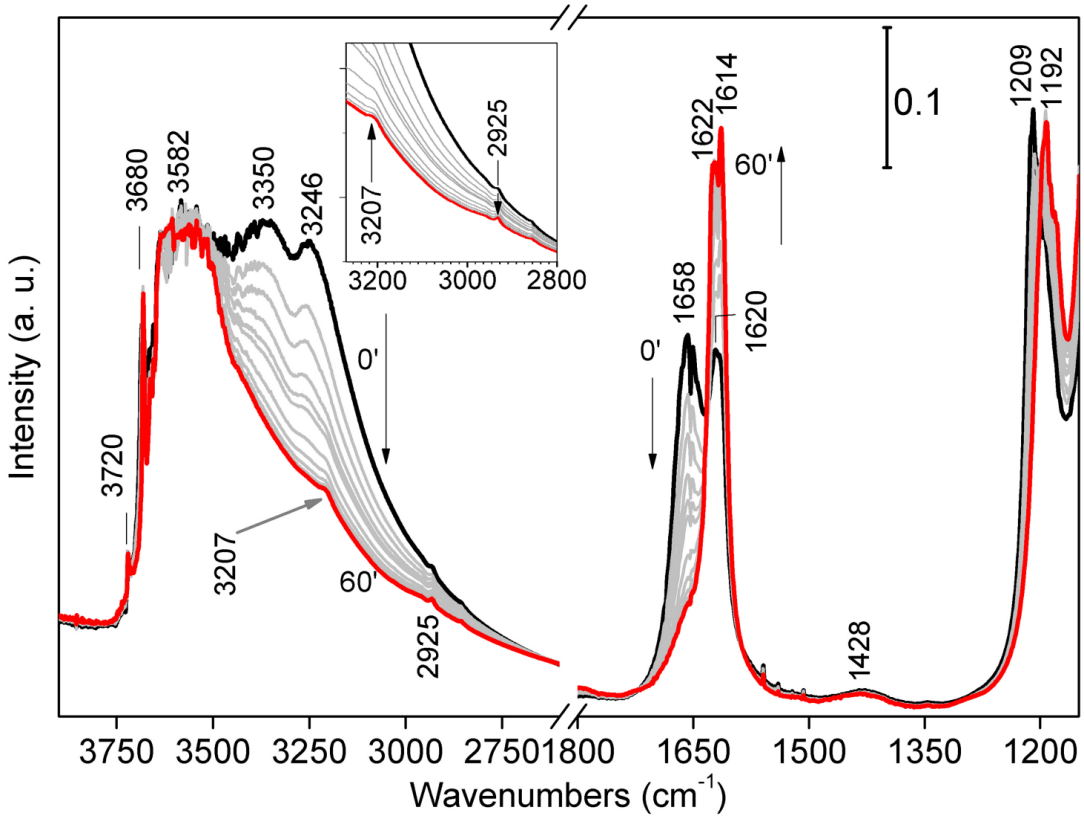
Intensity (a. u.)
Wavenumbers (cm-1)
3720
3680
3582
3350
3246
3207
2925
1658
1622
1614
1620
1428
1209
1192
0'
60'
0.1

Fig. 6

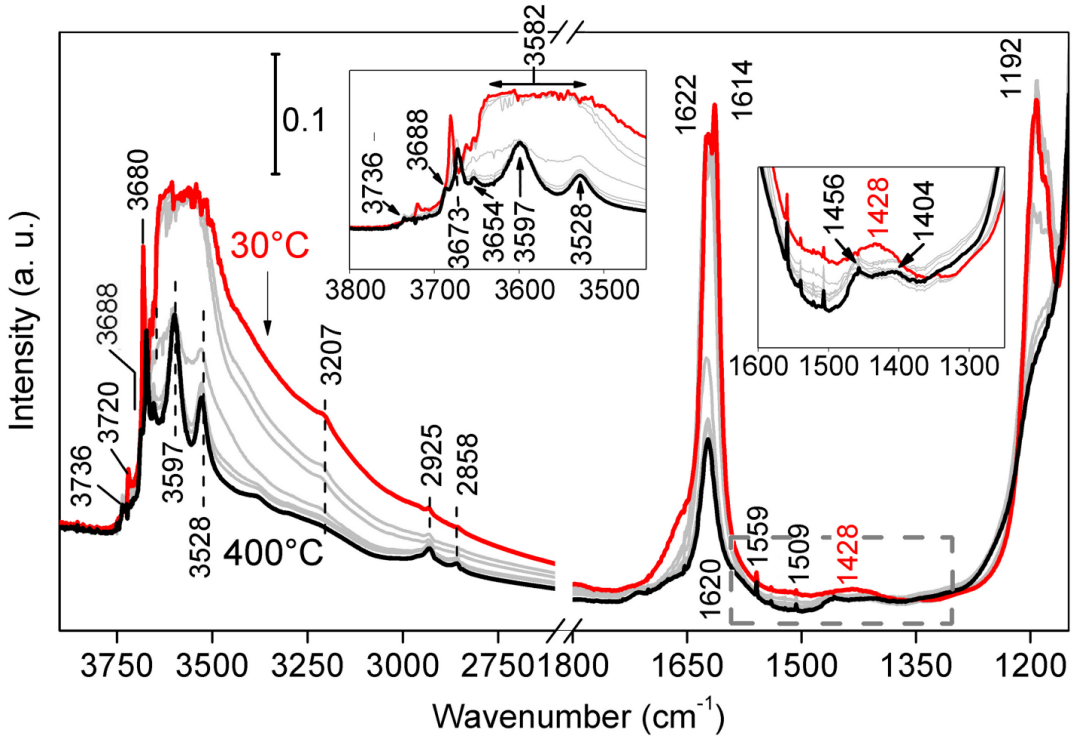
Intensity (a. u.)
Wavenumber (cm-1)
0.1
30°C
400°C
3582
3680
3688
3720
3736
3597
3528
3207
2925
2858
1622
1614
1192
1620
1559
1509
1428
1456
1404
3673
3654
3750 3500 3250 3000 2750
1800 1650 1500 1350 1200
3800 3700 3600 3500
1600 1500 1400 1300

Fig. 7

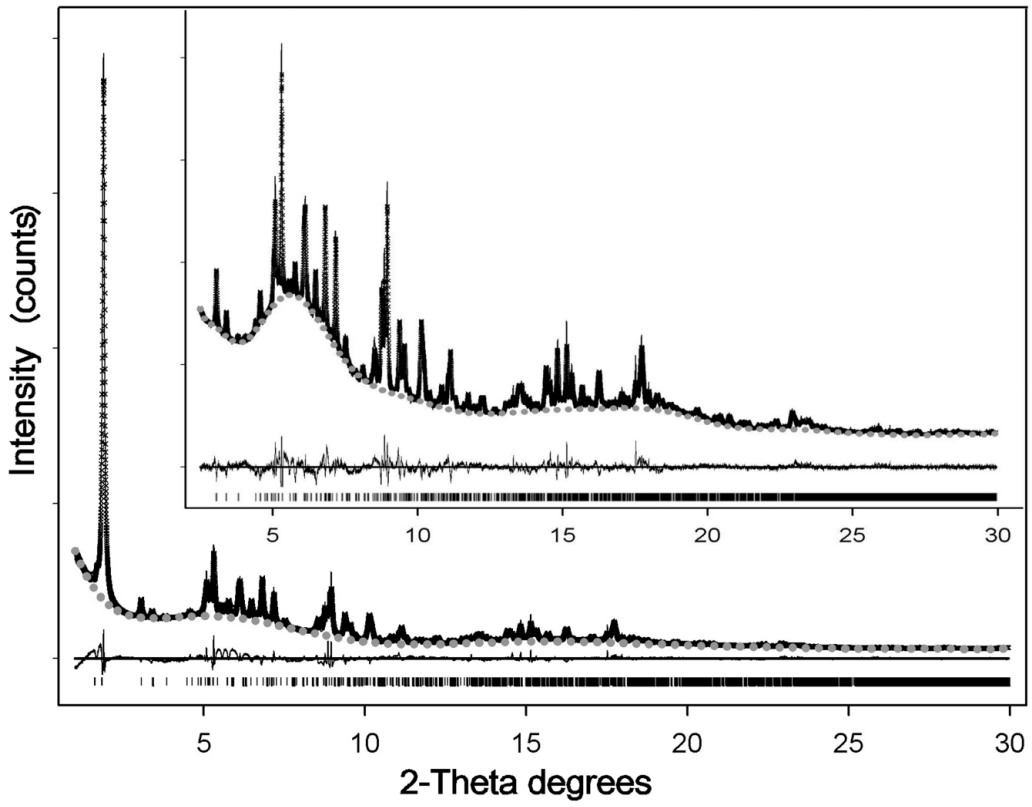
Intensity (counts)
2-Theta degrees
5 10 15 20 25 30

Fig. 8

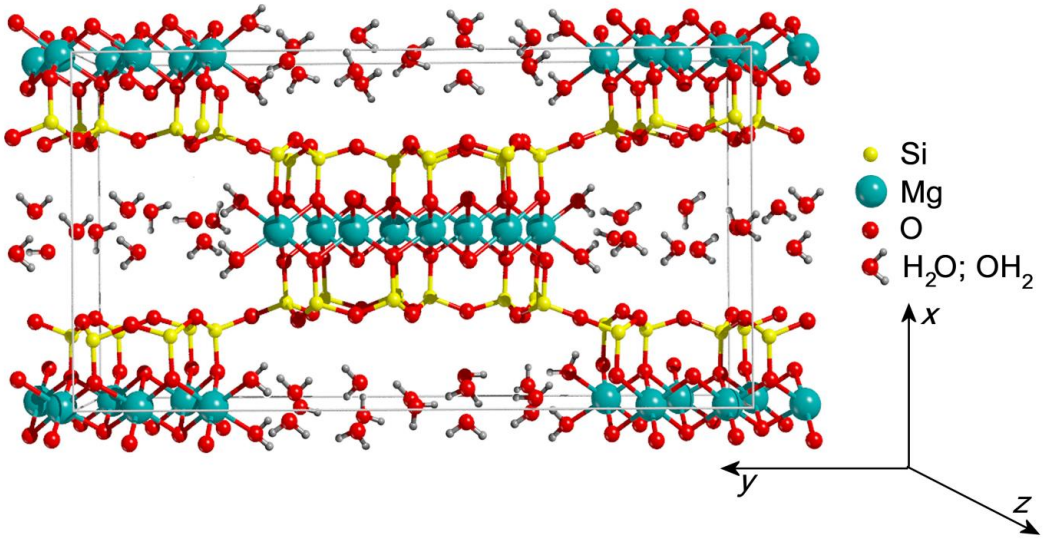

Fig. 9